CHEMISTRY
A EUROPEAN JOURNAL

ChemPubSoc Europe

DOI: 10.1002/chem.201204184

Probing the Coordination Environment of the Human Copper Chaperone HAH1: Characterization of Hg^{II}-Bridged Homodimeric Species in Solution

Marek Łuczkowski,[a, d] Brian A. Zeider,[b] Alia V. H. Hinz,[b] Monika Stachura,[c] Saumen Chakraborty,[a] Lars Hemmingsen,*[c] David L. Huffman,*[b] and Vincent L. Pecoraro*[a]

Abstract: Although metal ion homeostasis in cells is often mediated through metallochaperones, there are opportunities for toxic metals to be sequestered through the existing transport apparatus. Proper trafficking of Cu^{I} in human cells is partially achieved through complexation by HAH1, the human metallochaperone responsible for copper delivery to the Wilson and Menkes ATPase located in the trans-Golgi apparatus. In addition to binding copper, HAH1 strongly complexes Hg^{II}, with the X-ray structure of this complex previously described. It is important to clarify the solution behavior of these systems and, therefore, the binding of Hg^{II} to HAH1 was probed over the pH range 7.5 to 9.4 using ^{199}Hg NMR, ^{199m}Hg PAC and UV–visible spectroscopies. The metal-dependent protein association over this pH range was examined using analytical gel-filtration. It can be concluded that at pH 7.5, Hg^{II} is bound to a monomeric HAH1 as a two coordinate, linear complex (HgS_2), like the Hg^{II}–Atx1 X-ray structure (PDB ID: 1CC8). At pH 9.4, Hg^{II} promotes HAH1 association, leading to formation of HgS_3 and HgS_4 complexes, which are in exchange on the μs–ns time scale. Thus, structures that may represent central intermediates in the process of metal ion transfer, as well as their exchange kinetics have been characterized.

Keywords: ^{199m}Hg PAC · copper · mercury · metallochaperones · NMR spectroscopy

Introduction

Copper is an essential trace element that is present in all living organisms[1] being found in a number of metalloproteins that are crucial for a plethora of cellular processes ranging from biological electron transfer,[2] oxygen transport,[3] dioxygen activation,[4] and aerobic respiration.[5] Suitable redox potentials leading to the formation of stable Cu^{II} and Cu^{I} oxidation states with minimal geometrical perturbations makes copper an important element for the aforementioned biological processes. However, the formation of the stable Cu^{I} oxidation state poses a great danger in the cellular milieu due to the generation of extremely toxic hydroxyl radicals by Cu^{I}-catalyzed Fenton reactions.[6] For example, the human brain is estimated to produce more than 10^{11} free radicals per day.[7] Additionally, the highly soft character of Cu^{I} leads to the displacement of iron from iron–sulfur clusters of many enzymes.[8] Such deleterious effects are avoided by tight control of intracellular trafficking of copper by the utilization of metallochaperones, which ensure that the right metal is delivered to the target protein in a safe and secure manner.[9]

In humans there are four major routes of copper trafficking.[10] One of these involves binding of Cu^{I} to the copper chaperone HAH1 that has been implicated for the delivery of this metal ion to the Wilson and Menkes ATPase located in the trans-Golgi apparatus.[11] HAH1 consists of 68 amino acids and folds into an α/β sandwich structure. A conserved MT/H-C-X-X-C metal binding motif is located on the surface of HAH1 and at the N terminus of its target proteins. Although it is known that Cu^{I} binds to HAH1 via this motif, the comprehensive mechanism of copper transfer by HAH1 is not yet known. In vitro, HAH1 is capable of delivering copper to all six metal binding domains, but copper-dependent NMR-observable complexes only occur with metal binding domains one, two and four of the Wilson ATPase and metal binding domains one and four of the Menkes ATPase; however, single-molecule fluorescence resonance energy transfer experiments record simultaneous interactions between HAH1 with metal binding domains three and four of the Wilson ATPase.[12] Thus, metal binding domains

[a] Dr. M. Łuczkowski, Dr. S. Chakraborty, Prof. V. L. Pecoraro
Department of Chemistry, University of Michigan
Ann Arbor, MI 48109-1055 (USA)
E-mail: vlpec@umich.edu

[b] Dr. B. A. Zeider, A. V. H. Hinz, Dr. D. L. Huffman
Department of Chemistry, Western Michigan University
Kalamazoo, MI 49008-5413 (USA)
E-mail: david.huffman@wmich.edu

[c] Dr. M. Stachura, Prof. L. Hemmingsen
Department of Chemistry, University of Copenhagen
Universitetsparken 5, 2100 Copenhagen (Denmark)
E-mail: lhe@chem.ku.dk

[d] Dr. M. Łuczkowski
On leave from: Faculty of Chemistry, University of Wrocław
14 Joliot-Curie, 50-383 Wrocław (Poland)

Supporting information for this article is available on the WWW under http://dx.doi.org/10.1002/chem.201204184.

one through four function to capture copper from HAH1, whereas domains five and six appear to regulate the activity of the ATPase. X-ray structures of HAH1 with Cu^{I}, Hg^{II}, and Cd^{II} have been determined,[13] as well as the NMR structures of apo- and Cu^{I}-bound HAH1.[14] The X-ray structures of metallated HAH1 showed that the metals form 3- or 4-coordinate complexes with two HAH1 molecules forming a homodimer. However, the NMR studies show only a monomeric structure in which Cu^{I} is bound to two chelating Cys residues from the same protein molecule. Based on the dimeric structure determined by X-ray crystallography, Rosenzweig and co-workers proposed that the docking of $Cu^{I}S_2$-bound HAH1 monomer with the target protein via the conserved metal binding domains, followed by ligand exchange reactions leading to the formation of a three-coordinate intermediate in which the metal is bound to both proteins, completes the transfer of copper from the chaperone to the target protein.[13] This ligand exchange mechanism is supported by experiments between the yeast homologues, the metallochaperone Atx1 and the Ccc2 ATPase.[15] Furthermore, yeast Atx1 can transfer Hg^{II} to Ccc2, suggesting that Hg^{II} can be a model for Cu^{I}, and that the copper transfer machinery can sequester this toxic metal.[16]

Using a series of de novo designed parallel three-stranded coiled coil peptides [Ac-G(LKALEEK)$_x$-G-NH_2, $x=3$ for TRI, $x=4$ for GRAND] we have generated homoleptic thiol-rich binding sites for heavy metals, such as Hg^{II}, Cd^{II}, As^{III}, and Pb^{II}, by substitution of one or more Leu residues from the hydrophobic interior of these polypeptides.[17] These metallopeptides have served as excellent structural models for the metalloregulatory proteins, such as MerR, CmtR, and ArsR.[18] Peptides containing two Cys substitutions lacking intervening leucines between the sulfurs in the heptad (TRIL9L12C) formed a Hg^{II} complex with spectral features that resemble those of the metal center of Hg^{II}-bound rubredoxin.[19] Our studies based on Hg^{II} sequestration by these peptides have shown that raising the solution pH enforces the preference of the metal ion to a higher coordination number.[18a,e] Using our knowledge from these studies, in this work we have investigated the coordination geometry of Hg^{II} bound to HAH1 at different pH values.

The X-ray structure of Hg^{II}–HAH1 obtained at pH 6.5 showed coordination of Hg^{II} with three of the cysteine residues from the HAH1 homodimer (A_2B_2) with Hg^{II}–S distances of 2.3 Å (Cys A12), 2.5 Å (Cys A15), and 2.5 Å (Cys B12), whereas the fourth Cys (Cys B15) of the homodimer was at 2.8 Å away from the metal center, implying there was no bond between Cys B15 and Hg^{II}.[13]

Evaluation of the pH-dependent association state and Hg^{II}-binding properties of HAH1 would provide information on the coordination environment of the metal ion at the desired pH and help elucidate the observed variation in physiologically relevant structures. We hypothesize that at pH 6.5, Cys B15 is not deprotonated and hence is not directly bound to Hg^{II} and at high pH Cys B15 could be deprotonated to form a Hg^{II}–thiolate bond. In this work, we have investigated the oligomerization state and Hg^{II}-binding properties to HAH1 under various pH conditions to explore whether a dimeric Hg^{II}–$(HAH1)_2$ complex can be observed in solution, and whether Hg^{II} can form a four-coordinate HgS_4 structure with all four cysteines bound to the metal ion as thiolates employing a number of analytical techniques, such as ^{199}Hg NMR spectroscopy, ^{199m}Hg perturbed angular correlation of gamma rays spectroscopy (^{199m}Hg PAC), electronic spectroscopy, mass spectrometry and analytical gel filtration.

Results and Discussion

^{199}Hg NMR spectroscopy: Initial detection of Hg^{II}–HAH1 complexes in solution was done by ^{199}Hg NMR experiments. As the pH was increased there were definite changes in the chemical shifts (Figure 1). At physiological pH (~7.5)

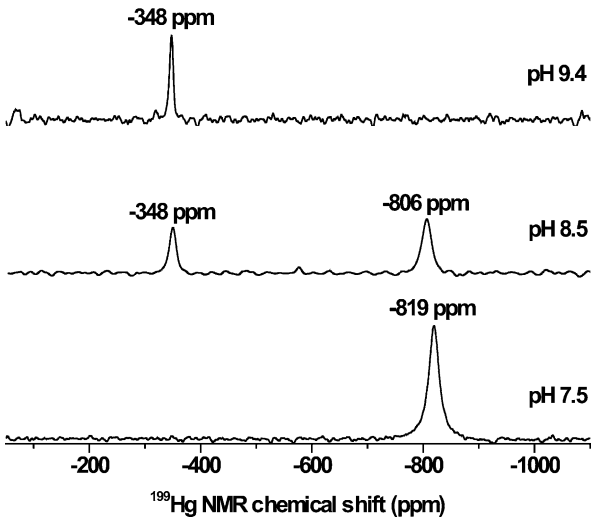

Figure 1. $^{199}Hg^{II}$ NMR spectra at various pH values, indicating a change in the coordination environment around the mercury(II).

$^{199}Hg^{II}$ NMR spectroscopy revealed a single peak at −819 ppm, which coincides with the chemical shift values obtained from 2-coordinate mercury(II) species.[20] O'Halloran's group showed a single chemical shift at −821 ppm indicative of a 2-coordinate mercury(II) thiolate species.[20a] When the pH was increased to 8.5, a second complex appears with a chemical shift of −348 ppm. This chemical shift falls within the range where 4-coordinate aliphatic mercury(II) thiolates are observed (−300 to −500 ppm).[21] MerR has a 3-coordinate environment and has chemical shifts of approximately −106 ppm.[20a] The range of chemical shift for a 3-coordinate mercury thiolate is reported to be from −80 to −160 ppm for trigonal planar species and around −360 ppm for distorted trigonal species.[20a,22] These assignments have recently been expanded using designed peptides in which crystallographic information proves that a ^{199}Hg NMR resonance of −185 ppm corresponds to a trigonal planar Hg^{II} bound to three cysteine thiolates.[23] Interest-

ingly, the crystal structure of the HAH1 dimer displays a HgS_3 coordination geometry with a fourth cysteine sulfur in close proximity (2.8 Å from the Hg^{II}). It is thus tempting to assume that the resonance at −348 ppm originates from this structure, accounting for the chemical shift being in the low range of four-coordinated and in range of three-coordinated distorted trigonal planar structures, vide supra.

^{199m}Hg perturbed angular correlation spectroscopy: The PAC experiments were carried out at the same pH values used in the ^{199}Hg NMR experiments (Figure 2). At pH 7.5 the PAC

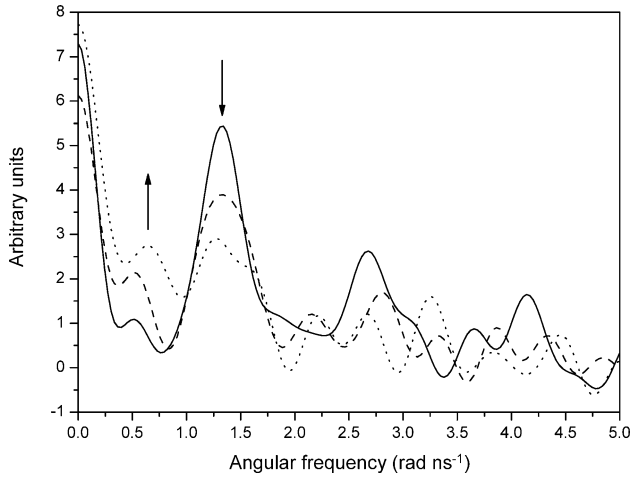

Figure 2. Fourier transform (FT) of the experimental ^{199m}Hg PAC data for HAH1 at pH 7.5 (solid line), 8.5 (dash line), and 9.4 (dotted line). The two major signals and their change with pH are indicated by the arrows. Samples contain 100 mM of the proper buffer, 200 μM HAH1, 100 μM of $HgCl_2$ and 55% w/w sucrose.

experiment gives one signal that compares well with literature data for a HgS_2 species,[19a] in agreement with the NMR spectroscopy data. At pH 8.5 the major peak (at ~1.4 rad ns^{-1}) still occupies the same position but its amplitude decreases by about one third, and it is broadened. In the same spectrum a new peak appears at lower frequency (~0.5 rad ns^{-1}) accounting for the loss of signal in the major peak. The lower frequency of this new signal indicates an increase in the coordination number, and it is comparable to literature data for distorted HgS_4 coordination geometries.[24] At pH 9.4 there are still unambiguously two (or more) NQIs present in the PAC data, as indicated by the arrows in Figure 2. These data appear to contradict the ^{199}Hg NMR spectroscopy data, where only one resonance is observed at high pH. A straight forward explanation for this observation is that the two species are in slow exchange on the PAC time scale (ns) but in fast exchange on the NMR time scale (ms). The low frequency PAC signal may reflect a HgS_4 structure, but the high frequency signal is more complex, and cannot be easily analyzed. The second and third peaks at approximately 2.7 and 4.1 rad ns^{-1}, which are clearly visible at pH 7.5, are not present beyond the noise at pH 9.4, and the major peak displays line broadening. This observation indicates that either: 1) ligand dynamics is occurring on the ns time scale leading to line broadening, or 2) another NQI with high η reflecting a structure different from a linear HgS_2 coordination geometry is present under this condition. The most obvious possibility is a T-shaped HgS_3 structure ($\eta = 1$ according to the BASIL model).[25] In a quantitative analysis (Table S4 in the Supporting Information), it appears that there may even be more than two NQIs present in the PAC data at pH 9.4, and this might reflect that both HgS_2, HgS_3, and HgS_4 co-exist in the metal ion bridged homodimer. However, there are several equally satisfactory fits of the data, and thus we are reluctant to put too much emphasis on this conclusion. We conclude that the signal at pH 9.4 most likely reflects an equilibrium between two (or more) species one of which is a distorted HgS_4 species and the other presumably a T-shaped HgS_3 species.

In summary, a model that accounts for all the NMR- and PAC-spectroscopic data is a linear HgS_2 coordination geometry under normal physiological conditions, but at higher pH this changes into two (or more) species with higher coordination number—most likely a HgS_4 and possibly a T-shaped HgS_3 species. The pK_a for the transition is about 8.5 for the NMR experimental conditions and comparable for the PAC experimental conditions.

The exchange dynamics between the pure linear HgS_2 species (−806 ppm) and the more complex mixture of species (−348 ppm) is slow on the NMR time scale at pH 8.5 (ms or slower) as both are observed with only minor line broadening in the NMR spectroscopy data. The exchange between the higher coordination number species at pH 9.4 is fast (μs–ns) on the NMR time scale, as they coalesce into one resonance in the NMR spectrum but are both observed in the PAC spectrum. These conclusions, taken together, imply that the metal ion transfer to the Wilson or Menkes ATPase occurs most effectively at a neutral pH, when the monomer is free to interact with its target; however, a structural change at higher pH, related to the deprotonation of the protein thiolates, favors a three or four coordinate Hg^{II}-bridged dimer. Intriguingly, the pH-dependent spectroscopic data indicate the presence of several species that mirror the transfer of Cu^{I} from HAH1 to the Wilson and Menkes ATPase—the reactant HgS_2 species, the initial encounter complex presumably forming a T-shaped HgS_3 species, and a distorted HgS_4 species which could be another intermediate in the metal transfer process. The latter may be the structure reported by X-ray diffraction studies.[13] The identification of these species confers with the model proposed by Wernimont et al.,[13] although the presence of a HgS_4 structure was not considered in the metal transfer scheme and HgS_4 may not be compatible with facile metal transfer. Other studies, between the metallochaperone and the ATPase metal binding domains, indicate that at least three thiolate ligands are required to trap a metal transfer intermediate.[15b,26]

Electronic spectroscopy: Information from ^{199}Hg NMR spectroscopy and ^{199m}Hg PAC allowed us to elucidate the pH dependence of coordination properties of HAH1. At the phys-

iological pH, Hg^{II} forms, in solution, a preferred digonal HgS_2 form. While pH increases, binding of further thiolate ligand(s) is observed.

To evaluate the findings of the previous two techniques further, UV/Vis spectroscopy measurements were performed to determine the metal-to-ligand charge transfer bands for mercury(II)–thiolate coordination at the different pH values (Figure 3A). The presence of the ligand-to-metal

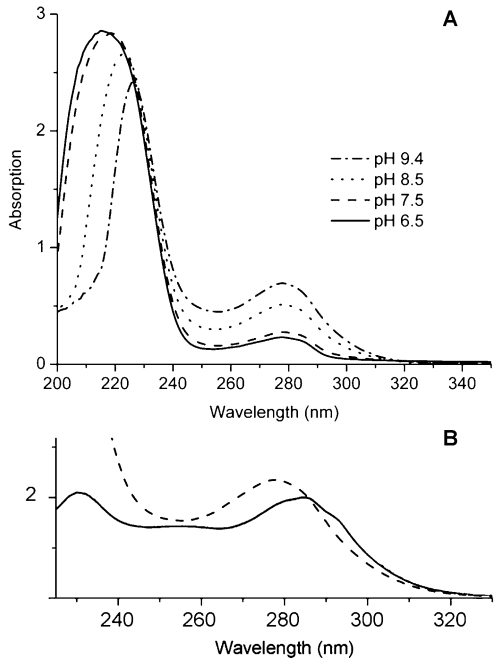

Figure 3. A) Electronic spectra of Hg^{II} complexes of HAH1 at different pH values, and B) comparison of spectra of Hg^{II} substituted rubredoxin at pH 8.0 (solid line) and Hg^{II} bound HAH1 at pH 9.4 (dotted line). [HAH1] = 60 μM and [Hg^{II}] = 30 μM in phosphate buffer (50 mM) at pH 6.5, 7.5, 8.5 and CHES buffer (50 mM) at pH 9.4, respectively.

charge transfer band at 278 nm ($\Delta\varepsilon = 23\,100\ M^{-1}cm^{-1}$ at pH 9.4) indicates the formation of HgS_4 or T-shaped HgS_3 rather than a trigonal planar HgS_3 complex, further corroborating the ^{199}Hg NMR spectroscopy data.[19b] Interestingly, an analogous electronic transition has been reported for mercury substituted rubredoxin (Figure 3B).[24b] An additional peak at around 220 nm corresponds to a S→Hg^{II} charge transfer band of a linear Hg^{II} complex species.

Association state studies based on pH titrations; gel filtration analysis: Although the coordination number of Hg^{II} in HAH1 complexes at various pH values has been elucidated with the application of spectroscopic techniques, the driving force of observed changes has not been determined. Therefore, we performed gel filtration assays to determine apparent masses and the association state of the HAH1 and its Hg^{II} complexes. This information would verify whether the observed changes of coordination number of the detected species are a consequence of ligand- or metal-driven processes. Figure 4 shows the elution profiles of apo-HAH1 and Hg^{II}–HAH1 samples at three different pH values. For Hg^{II}–HAH1, a pH increase is correlated with the increase of detected mass, indicating a higher order complex in contrast to the apo-protein, which appears to remain monomeric at all pH values investigated.

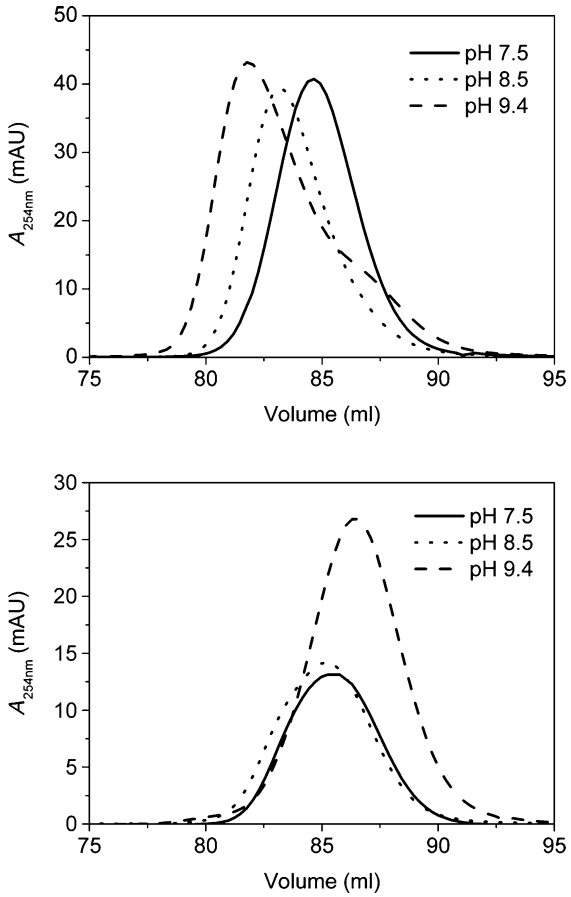

Figure 4. Gel filtration curves showing the elution profiles from a Superdex 75 HiLoad 16/600 column (pH range 7.5–9.4) for Hg^{II}–HAH1 (top) and apo-HAH1 (bottom). The top curve indicates that as the pH increases, Hg^{II}–HAH1 begins to dimerize. (Note: the shoulder appearing at approximately 85 mL at pH 9.4 in the Hg^{II}–HAH1 curve is likely apo-HAH1 monomer, since this is where the monomer elutes at this pH.) The same amount of apo-HAH1 and Hg^{II}–HAH1 was loaded for all injections. The increase in absorbance of apo-HAH1 at pH 9.4 may be due to the partial deprotonation of tyrosine.[27] Samples for gel filtration experiments were prepared in phosphate buffer (100 mM), NaCl (200 mM), TCEP (1 mM) for pH values 7.5 and 8.5, and CHES (100 mM), NaCl (200 mM), TCEP (1 mM) for pH 9.4.

Table S3 in the Supporting Information shows the apparent masses of each of the metal-bound species. At pH 7.5, the apparent mass of Hg^{II}–HAH1 (9.7 kDa) was consistent with the mass of apo-HAH1 (9.5 kDa), indicating that Hg^{II}–HAH1 was monomeric at this pH. As the pH increased to 8.5, however, the apparent mass of Hg^{II}–HAH1 increased to 10.5 kDa while the apparent mass of apo-HAH1 remained at 9.5 kDa. In the NMR spectroscopy data there was strong evidence for two different species existing at the latter pH;

however, due to the conditions of the gel filtration study, these two species could not be resolved. The apparent mass of Hg^{II}–HAH1 at pH 9.4 increased to 11.4 kDa, providing further evidence that homodimerization is increasing with increasing pH. Curiously, the apparent mass of apo-HAH1 at pH 9.4 decreased to 8.3 kDa; this decrease may be due to the protein adopting a molten globule conformation at this pH and becoming more compact. Circular dichroism spectra in the far UV region (data not shown) did not reveal any substantial changes in the secondary structure between apo-HAH1 at pH values 8.5 and 9.4. This suggests that while apo-HAH1 at pH 9.4 has the same secondary structure as apo-HAH1 at pH 8.5, the tertiary structure may be altered.[28]

Mass spectrometry: The results of the mass spectrometric analyses are consistent with the gel filtration findings and indicate that at slightly acidic pH conditions HAH1 and its mercurated complex exist in the protein's monomeric aggregation state. The ESI-MS spectra recorded for solutions containing twofold molar excess of protein with respect to Hg^{II} revealed the presence of peaks corresponding to the monomer of apo-protein (*m*/*z* 1246.4), monomer of holo-protein (*m*/*z* 1279.8) and the monomer of the chlorinated adduct of the former one (*m*/*z* 1257.5; Figure 5). Furthermore, the

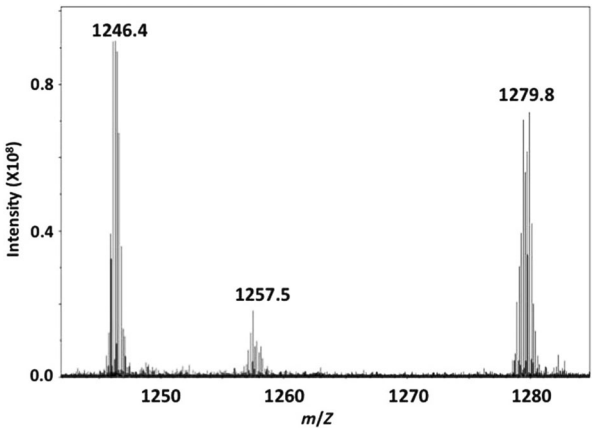

Figure 5. ESI-MS spectra of Hg^{II} complex of HAH1 at pH 6.5 in carbonate buffer (1 mM). [HAH1] = 1×10^{-4} M; Hg^{II}/HAH1 ratio 1:2; MeOH/H_2O = 50:50.

first two peaks were of comparable intensities, indicating a 50:50 ratio between apo- and holo- forms of the protein.

The MS analysis performed for the samples at high pH adjusted with CHES buffer (data not shown) gave no results due to protein spectra suppression.

Combining conclusions on protein structure and metal coordination environment: Although the previously reported crystal structure of the Hg^{II}–HAH1 dimer provided critical structural insight on Hg^{II} binding to this metallochaperone it could neither fully discriminate 3-coordinate from distorted 4-coordinate binding modes of Hg^{II} nor provide information on the exchange rates between the different species. The involvement of the fourth thiolate donor in the metal ion binding was questionable as the relatively long distance was inconsistent with bond formation. In addition, detailed solution data regarding the metal coordination environment has been lacking. The results of spectroscopic and association state experiments allow us to follow the changes of both coordination number and protein aggregation state that resulted from pH changes in solution. Thus, we can address whether similar species are present when the Hg^{II}–HAH1 system is in solution and possibly clarify the coordination environment of the metal. The NMR spectroscopy data and the ^{199m}Hg PAC experiments at low pH clearly indicate a single, 2-coordinate species that likely is structurally identical to the complex previously published by the O'Halloran group for the ATX1 protein.[20a] The incidence of the 2-coordinate Hg^{II}–ATX1 protein species yielded a peak at −821 ppm in the ^{199}Hg NMR spectrum, which is very close to the chemical shift observed in the present study for the human homologue HAH1 with the chemical shift of −819 ppm.[20a] As the pH was increased, a second ^{199}Hg NMR peak emerged at −348 ppm. This chemical shift value falls within the range characteristic for either a T-shaped 3-coordinate HgS_3 structure or a 4-coordinate HgS_4 complex. However, the ^{199}Hg NMR spectroscopy data alone do not definitively confirm the presence of these two species. Finally, at pH 9.5 a single peak at −348 ppm is observed, again consistent with either 3- or 4-coordinate species. Similar conclusions could be drawn for the UV/Vis spectroscopic data, although the spectra can be interpreted to discriminate in favor of the 4-coordinate species.

Application of PAC spectroscopy resolved this ambiguity, illustrating that the fourth sulfur donor might be close enough to be coordinated to the Hg^{II} at high pH. Analysis of the PAC data unambiguously demonstrate the presence of two (or more) species at pH 9.4; one signal originating from a distorted 4-coordinate HgS_4 structure, and another which according to the BASIL model agrees with a T-shaped 3-coordinate structure.

Figure 6 provides pictorially our present understanding of this system. At neutral pH, a monomeric HgS_2 complex exists. At higher pH a dimeric HAH1 forms yielding a mixture of T-shaped HgS_3 and distorted HgS_4 structures.

Next, we addressed the question as to whether the protein association was driven by Hg^{II} coordination or whether it was simply protein dependent. The gel filtration analysis performed with the holo-protein revealed that it exists as a monomer at neutral pH, and that an increase in pH led to protein association in a metal-dependent manner. In contrast, the elution profile for the apo-protein indicated that the protein remained monomeric at the various pH values (the slight decrease in the apparent mass that was observed at pH 9.4 may be due to the protein adopting a molten globule structure). These data conclusively demonstrate that the observed protein association at higher pH is induced by metal complexation. It is important to note that no HAH1

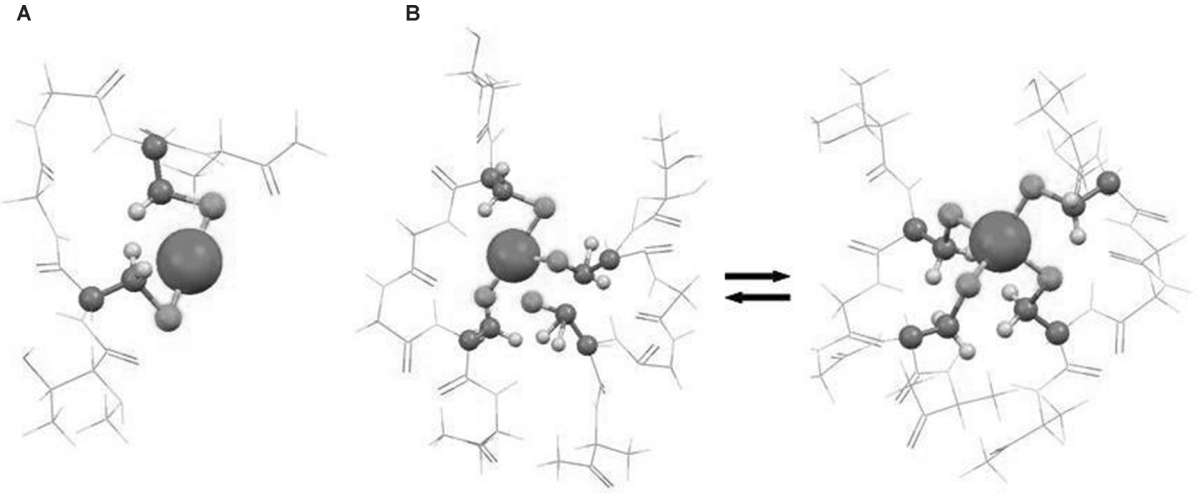

Figure 6. Generic graphical representation of Hg^{II}–HAH1 species formed at: A) pH 7.5 (linear HgS_2) and B) pH 9.4 (equilibrium between T-shaped HgS_3 and 4-coordinate HgS_4 species). Figure 6B is not intended to specify the precise cysteinyl residues involved in metal binding. Protein backbone is shown as lines. Hg^{II} is shown as gray big sphere, Cys side chains are shown as ball and stick representations with sulfurs being shown as light gray small spheres. The Figures were drawn in CS ChemOffice 2002 software package. Final Figure conversion was made in Mercury.

dimer has been found in the physiological pH range either for Hg^{II}–HAH1 or apo-HAH1.

The crystal structure of the dimerized Hg^{II}–HAH1 shows the lowest energy structure as HgS_3 or HgS_4, which may not be the best representation of the state of the complex in solution. In fact, within the physiological pH range the protein behaves as a monomer with a 2-coordinate Hg^{II}–thiolate environment. The results reported in this work clearly indicate that HAH1 can form 4-coordinate Hg^{II} complexes in solution; however, this occurs only at pH values higher than physiological conditions. Nevertheless, these higher coordination number species may be important to understanding metal ion transfer between proteins in the physiologic pH milieu.

One particularly intriguing aspect of metal transfer dynamics in this system is the observation that there is a rapid interconversion between the HgS_3 and HgS_4 structures. The process must be faster than the NMR timescale (hence submillisecond) but slower than the timescale of PAC (slower than nanoseconds). From this study we can now assign a range of timescale on Hg^{II}–thiolate exchange reactions occurring within this native protein. Furthermore, we can conclude that either a 3- or 4-coordinate species can exist during Hg^{II} exchange processes. This raises the intriguing question of Hg^{II} sequestration in humans. Fast transfer kinetics observed for specific protein–protein interactions may favor certain pathways of metal ion trafficking, overcoming thermodynamic hierarchy of directions.[29] For this reason, HAH1 may represent a plausible pathway of mercury trafficking as an important part of cell's detoxification pathways, as it may overcome the trapping effect of metallothioneins that can thermodynamically regulate the cellular distribution of metal ions. Such issues could be important for the molecular basis of Hg^{II} toxicity.

In conclusion, it is interesting that fundamental insight on Hg^{II} thiolate complexes garnered from de novo protein design studies can lead to formulable hypotheses that enhance our understanding of natural metal trafficking in human cells. In this case, we can see that a wide variety of coordination environments can be identified which follow the general observations reported with much simpler designed systems.

Experimental Section

Protein expression and purification: The HAH1 gene was synthesized from a series of overlapping primers, cloned into the vector pET11d and transformed into *E. coli* BL21(DE3) competent cells. The protein sequence begins with MAPKHE and ends with SYLGLE, thereby possessing an additional Ala at the beginning of the sequence relative to native HAH1. Protein expression was induced with IPTG (1 mM) at OD approximately 0.6 in LB medium for 3 h, then the cells were harvested. Bacterial cell pellets were subjected to three cycles of freeze-thaw followed by extracting the protein in the extraction buffer (20 mM MES, 1 mM EDTA, pH 5.5). After centrifugation, the supernatant was loaded onto a tandem set-up of an anion exchange column (diethylaminoethyl sepharose/DEAE; GE Healthcare) followed by a cation exchange column (carboxymethyl sepharose/CM; GE Healthcare) preequilibrated with binding buffer (20 mM MES, pH 6) and washed with approximately 20 column volume (CV) of the same buffer to remove unbound proteins from the columns. The DEAE column was used as a trap to bind most of the other contaminant proteins. The HAH1 protein was eluted from the CM column using a linear gradient of the elution buffer (20 mM MES, 1 M NaCl, pH 6) over approximately 10 CV. The eluted apo-protein was then further purified in a Superdex 75 (26/60) gel filtration column (GE Healthcare) preequilibrated with phosphate buffer (50 mM) containing NaCl (150 mM) at pH 7.5, and the purity was tested to be >95% by SDS-PAGE, reverse phase HPLC, and ESI-MS revealed a molar mass of 7478.4 (calcd 7472.7).[30]

^{199}Hg NMR spectroscopy: ^{199}Hg NMR spectra were collected at room temperature on a Varian Inova 500 MHz spectrometer tuned to 89.48 MHz for ^{199}Hg and equipped with a 5 mm broadband probe. A sol-

ution of $Hg(ClO_4)_2$ (0.1 mM) prepared in 0.1 mM $HClO_4/D_2O$ was used as an external standard, and had a chemical shift of −2250 ppm.[31] The NMR samples were prepared under a flow of argon by adding 10–15 mg of lyophilized HAH1 to a 15% solution of D_2O, and the concentration of protein was determined by Ellman's test.[32] The Hg^{II} was then added as $^{199}Hg(NO_3)_2$ in appropriate amounts to equate to one-half equivalent of the protein concentration followed by adjustment of pH to the desired value using concentrated solutions of KOH or HCl. A stock solution of $^{199}Hg(NO_3)_2$ (125 mM) was prepared by dissolving 91% isotopically enriched ^{199}HgO (Oak Ridge National Laboratory) in nitric acid. The ^{199}Hg NMR spectroscopy data were analyzed by using the software MestRe-C.[33] All free induction decays (FIDs) were zero filled to double the original points and processed by application of 200 Hz line broadening prior to Fourier transformation.

$^{199m}Hg^{II}$ perturbed angular correlation (PAC) spectroscopy: Perturbed angular correlation experiments were conducted to determine the coordination environment around the Hg^{II} bound to HAH1. These experiments were done at ISOLDE-CERN (Geneva, Switzerland). The protein was prepared by resuspending lyophilized HAH1 into either phosphate buffer (150 mM, pH 7.5 and 8.5) or CHES buffer (200 mM, pH 9.4). The following stock solutions were prepared and used for the PAC experiments: HAH1 (3 mM, concentration determined by the Ellman's test),[32] CHES buffer (1 M, pH 9.4), phosphate buffer (1 M) pH 6.3 (0.93 M for samples at pH 7.5, 8.5), and $HgCl_2$ (5.0 mM). The final samples contained the proper buffer (100 mM), HAH1 (200 μM), $HgCl_2$ (100 μM) and sucrose (55% w/w). The $^{199m}Hg^{II}$ was produced by irradiating the liquid lead target with 1.4 GeV protons, followed by using the online separation techniques at ISOLDE/CERN to select the proper isotope. Water (150 μL) was frozen in a Teflon cup using liquid nitrogen. The sample holder was then mounted in a vacuum chamber at the end of the beamline for collecting radioactive $^{199m}Hg^{I}$ (decays by the emission of two gamma rays with $T_{1/2}=43$ min for the first and 2.3 ns for the second). The ice was then thawed slowly (~10 min) in a fume hood under argon to prevent condensation of water vapor from the air. $HgCl_2$ (5 mM) solution was added, followed by 20 μL of appropriate buffer, and finally the protein, to get a protein to Hg ratio of 2:1. Since PAC measurements were done at 1 °C, the pH of the solutions was adjusted using concentrated solutions of KOH and HCl to the desired pH values correcting for the temperature dependence of phosphate and CHES buffers using the website: http://www.liv.ac.uk/buffers/buffercalc.html. After adjusting the pH, samples were left to equilibrate for 10 min, and finally sucrose was added to 55%. The sucrose was added to slow the tumbling of proteins due to Brownian motion.

The PAC instrument consisted of a 6-detector PAC camera set-up,[34] and data collection and analysis were done with Prelude and Winfit software (developed by Butz et al.) with a standard chi-square algorithm. Each nuclear quadruple interaction (NQI) was modeled using a different set of parameters (ν_Q, η, δ, τ_c and A); ν_Q is defined in Equation (1), where Q is the electric quadrupole moment of the Hg nucleus in the intermediate state of the nuclear decay, and V_{ZZ} represents the largest Eigenvalue of the electric field gradient (EFG) tensor.

$$\nu_Q = \frac{eQV_{ZZ}}{h} \quad (1)$$

The parameter η represents the asymmetry of the EFG (attaining a value of 0 in axially symmetric system, and values up to 1 in a highly asymmetrical system), δ is the relative frequency spread, τ_c is the rotational correlation time, and A is the amplitude of the signal.[25,35]

UV/Vis spectroscopy: UV/Vis spectra were collected on a Cary 100 Bio spectrophotometer with solutions containing HAH1 (60 μM) and Hg^{II} (30 μM) in phosphate buffer (50 mM) at pH 6.5, 7.5, 8.5 and CHES buffer (50 mM) at pH 9.4, respectively. In each case difference spectra were obtained by subtracting the spectra of solutions without added metal (60 μM protein in 50 mM phosphate or CHES buffer at the respective pH values). Difference molar absorptivities ($\Delta\varepsilon$, $M^{-1}cm^{-1}$) were calculated using total metal concentrations.

Analytical gel filtration experiments: Samples for gel filtration experiments were prepared in 100 mM phosphate buffer, 200 mM NaCl, 1 mM TCEP for pH values 7.5 and 8.5, and 100 mM CHES, 200 mM NaCl, 1 mM TCEP for pH 9.4. TCEP was included to maintain the HAH1 in the reduced state, as cysteine residues are prone to oxidation as pH increases, which could result in HAH1 dimerization. The purified apo-protein was concentrated using ultrafiltration. Protein concentration was determined using the Bradford assay (Bio-Rad). The Hg^{II}–HAH1 samples were prepared by adding 0.5 equivalents of Hg^{II} (in the form of $HgCl_2$) to reduced aliquots of HAH1.

The protein was injected on an ÄKTA FPLC (GE Healthcare) equipped with a Superdex 75 HiLoad 16/600 gel filtration column. The column was equilibrated with 1 CV (~120 mL) of the appropriate buffer and pH (Table S1 in the Supporting Information for buffer compositions) using a flow-rate of 1.0 mL min^{-1}. All the protein standards and HAH1 samples were analyzed under equivalent conditions. The apex of the peak was used as the elution volume of the protein, which was determined using the Unicorn software provided with the ÄKTA instrument. A mixture of protein standards (Table S2 in the Supporting Information) was injected at each pH and used to construct a calibration curve. These calibration curves were used to determine the apparent masses of apo- and Hg^{II}–HAH1 at each pH.

Mass spectrometry: High-resolution mass spectra were obtained on a BrukerQ-FTMS spectrometer equipped with an Apollo II electrospray ionization source with an ion funnel. The mass spectrometer was operated in the positive ion mode with the following parameters: scan range m/z 400–1600, dry gas-nitrogen, temperature 170 °C, ion energy 5 eV. Capillary voltage was optimized to 4500 V to obtain the highest S/N ratio. The small changes of voltage (±500 V) did not significantly affect the optimized spectra. The samples (metal/ligand in a 1:2 stoichiometry, $[ligand]=1\times10^{-4}$ M) were prepared in 1:1 MeOH/H_2O mixture at pH 6.5. Variation of the solvent composition down to 5% of MeOH did not change the speciation. The sample was infused at a flow-rate of 3 μL min^{-1}. The instrument was calibrated externally with the Tunemix™ mixture (Bruker Daltonik, Germany) in quadratic regression mode. Data were processed by using the Bruker Compass Data Analysis 4.0 program. The mass accuracy for the calibration was higher than 5 ppm, enabling together with the true isotopic pattern (SigmaFit) an unambiguous confirmation of the elemental composition of the obtained complex.

Acknowledgements

V.L.P. thanks the NIH (ES012236) for financial support. L.H. appreciates support from ISOLDE/CERN for beam time grants IS448 and IS488 and EURONS, The Danish Council for Independent Research, Natural Sciences, and the University of Copenhagen. D.L.H. acknowledges the National Science Foundation (Grant CAREER 0645518).

[1] a) C. Andreini, L. Banci, I. Bertini, A. Rosato, *J. Proteome Res.* **2008**, *7*, 209–216; b) Y. Zhang, V. N. Gladyshev, *Chem. Rev.* **2009**, *109*, 4828–4861; c) Y. Zhang, V. N. Gladyshev, *J. Biol. Chem.* **2010**, *285*, 3393–3405; d) Y. Zhang, V. N. Gladyshev, *J. Biol. Chem.* **2011**, *286*, 23623–23629.

[2] a) H. B. Gray, B. G. Malmstrom, R. J. P. Williams, *J. Biol. Inorg. Chem.* **2000**, *5*, 551–559; b) Y. Lu, in *Comprehensive Coordination Chemistry II* (Ed.: A. B. P. Lever), Pergamon, Oxford, **2003**, pp. 91–122; c) E. I. Solomon, *Inorg. Chem.* **2006**, *45*, 8012–8025; d) A. Vila, C. Fernandez, in *Copper in Electron-Transfer Proteins* (Eds.: I. Bertini, A. Sigel, H. Sigel), Marcel Dekker, New York, **2001**, pp. 813–856.

[3] E. Jaenicke, H. Decker, *ChemBioChem* **2004**, *5*, 163–169.

[4] M. R. Parsons, M. A. Convery, C. M. Wilmot, K. D. S. Yadav, V. Blakely, A. S. Corner, S. E. V. Phillips, M. J. Mcpherson, P. F. Knowles, *Structure* **1995**, *3*, 1171–1184.

[5] J. P. Hosler, S. Ferguson-Miller, D. A. Mills, *Annu. Rev. Biochem.* **2006**, *75*, 165–187.
[6] B. Halliwell, J. M. Gutteridge, *Methods Enzymol.* **1990**, *186*, 1–85.
[7] G. Perry, L. M. Sayre, C. S. Atwood, R. J. Castellani, A. D. Cash, C. A. Rottkamp, M. A. Smith, *CNS Drugs* **2002**, *16*, 339–352.
[8] L. Macomber, J. A. Imlay, *Proc. Natl. Acad. Sci. USA* **2009**, *106*, 8344–8349.
[9] a) A. K. Boal, A. C. Rosenzweig, *Chem. Rev.* **2009**, *109*, 4760–4779; b) D. L. Huffman, T. V. O'Halloran, *Annu. Rev. Biochem.* **2001**, *70*, 677–701; c) E. H. Kim, C. Rensing, M. M. McEvoy, *Nat. Prod. Rep.* **2010**, *27*, 711–719; d) T. V. O'Halloran, V. C. Culotta, *J. Biol. Chem.* **2000**, *275*, 25057–25060; e) N. J. Robinson, D. R. Winge, *Annu. Rev. Biochem.* **2010**, *79*, 537–562; f) S. Tottey, D. R. Harvie, N. J. Robinson, *Acc. Chem. Res.* **2005**, *38*, 775–783; g) S. Tottey, C. J. Patterson, L. Banci, I. Bertini, I. C. Felli, A. Pavelkova, S. J. Dainty, R. Pernil, K. J. Waldron, A. W. Foster, N. J. Robinson, *Proc. Natl. Acad. Sci. USA* **2012**, *109*, 95–100; h) K. J. Waldron, N. J. Robinson, *Nat. Rev. Microbiol.* **2009**, *7*, 25–35.
[10] H. Shim, Z. L. Harris, *J. Nutr.* **2003**, *133*, 1527S–1531S.
[11] I. Hamza, M. Schaefer, L. W. J. Klomp, J. D. Gitlin, *Proc. Natl. Acad. Sci. USA* **1999**, *96*, 13363–13368.
[12] a) L. Banci, I. Bertini, F. Cantini, N. Della-Malva, M. Migliardi, A. Rosato, *J. Biol. Chem.* **2007**, *282*, 23140–23146; b) L. Banci, I. Bertini, F. Cantini, C. Massagni, M. Migliardi, A. Rosato, *J. Biol. Chem.* **2009**, *284*, 9354–9360; c) L. Banci, I. Bertini, F. Cantini, A. C. Rosenzweig, L. A. Yatsunyk, *Biochemistry* **2008**, *47*, 7423–7429; d) A. M. Keller, J. J. Benítez, D. Klarin, L. Zhong, M. Goldfogel, F. Yang, T.-Y. Chen, P. Chen, *J. Am. Chem. Soc.* **2012**, *134*, 8934–8943.
[13] A. K. Wernimont, D. L. Huffman, A. L. Lamb, T. V. O'Halloran, A. C. Rosenzweig, *Nat. Struct. Biol.* **2000**, *7*, 766–771.
[14] I. Anastassopoulou, L. Banci, I. Bertini, F. Cantini, E. Katsari, A. Rosato, *Biochemistry* **2004**, *43*, 13046–13053.
[15] a) F. Arnesano, L. Banci, I. Bertini, F. Cantini, S. Ciofi-Baffoni, D. L. Huffman, T. V. O'Halloran, *J. Biol. Chem.* **2001**, *276*, 41365–41376; b) L. Banci, I. Bertini, F. Cantini, I. C. Felli, L. Gonnelli, N. Hadjiliadis, R. Pierattelli, A. Rosato, P. Voulgaris, *Nat. Chem. Biol.* **2006**, *2*, 367–368.
[16] A. C. Rosenzweig, D. L. Huffman, M. Y. Hou, A. K. Wernimont, R. A. Pufahl, T. V. O'Halloran, *Struct. Fold. Des.* **1999**, *7*, 605–617.
[17] a) G. R. Dieckmann, D. K. McRorie, J. D. Lear, K. A. Sharp, W. F. DeGrado, V. L. Pecoraro, *J. Mol. Biol.* **1998**, *280*, 897–912; b) B. T. Farrer, N. P. Harris, K. E. Balchus, V. L. Pecoraro, *Biochemistry* **2001**, *40*, 14696–14705; c) B. T. Farrer, C. P. McClure, J. E. Penner-Hahn, V. L. Pecoraro, *Inorg. Chem.* **2000**, *39*, 5422–5423; d) B. T. Farrer, V. L. Pecoraro, *Proc. Natl. Acad. Sci. USA* **2003**, *100*, 3760–3765; e) O. Iranzo, T. Jakusch, K. H. Lee, L. Hemmingsen, V. L. Pecoraro, *Chem. Eur. J.* **2009**, *15*, 3761–3772; f) M. Matzapetakis, D. Ghosh, T. C. Weng, J. E. Penner-Hahn, V. L. Pecoraro, *J. Biol. Inorg. Chem.* **2006**, *11*, 876–890; g) M. Matzapetakis, V. L. Pecoraro, *J. Am. Chem. Soc.* **2005**, *127*, 18229–18233; h) K. P. Neupane, V. L. Pecoraro, *Angew. Chem.* **2010**, *122*, 8353–8356; *Angew. Chem. Int. Ed.* **2010**, *49*, 8177–8180; i) K. P. Neupane, V. L. Pecoraro, *J. Inorg. Biochem.* **2011**, *105*, 1030–1034.
[18] a) G. R. Dieckmann, D. K. Mc Rorie, D. L. Tierney, L. M. Utschig, C. P. Singer, T. V. O'Halloran, J. E. Penner Hahn, W. F. De Grado, V. L. Pecoraro, *J. Am. Chem. Soc.* **1997**, *119*, 6195–6196; b) D. Ghosh, K. H. Lee, B. Demeler, V. L. Pecoraro, *Biochemistry* **2005**, *44*, 10732–10740; c) D. Ghosh, V. L. Pecoraro, *Curr. Opin. Chem. Biol.* **2005**, *9*, 97–103; d) M. Matzapetakis, B. T. Farrer, T. C. Weng, L. Hemmingsen, J. E. Penner-Hahn, V. L. Pecoraro, *J. Am. Chem. Soc.* **2002**, *124*, 8042–8054; e) V. L. Pecoraro, A. F. A. Peacock, O. Iranzo, M. Luczkowski, *ACS Symp. Ser.* **2009**, *1012*, 183–197; f) D. S. Touw, C. E. Nordman, J. A. Stuckey, V. L. Pecoraro, *Proc. Natl. Acad. Sci. USA* **2007**, *104*, 11969–11974; g) G. Zampella, K. P. Neupane, L. De Gioia, V. L. Pecoraro, *Chem. Eur. J.* **2012**, *18*, 2040–2050.
[19] a) O. Iranzo, P. W. Thulstrup, S. B. Ryu, L. Hemmingsen, V. L. Pecoraro, *Chem. Eur. J.* **2007**, *13*, 9178–9190; b) M. Luczkowski, M. Stachura, V. Schirf, B. Demeler, L. Hemmingsen, V. L. Pecoraro, *Inorg. Chem.* **2008**, *47*, 10875–10888.
[20] a) R. A. Pufahl, C. P. Singer, K. L. Peariso, S. J. Lin, P. J. Schmidt, C. J. Fahrni, V. C. Culotta, J. E. Penner Hahn, T. V. O'Halloran, *Science* **1997**, *278*, 853–856; b) G. Veglia, F. Porcelli, T. DeSilva, A. Prantner, S. J. Opella, *J. Am. Chem. Soc.* **2000**, *122*, 2389–2390.
[21] S. P. Watton, J. G. Wright, F. M. Macdonnell, J. W. Bryson, M. Sabat, T. V. O'Halloran, *J. Am. Chem. Soc.* **1990**, *112*, 2824–2826.
[22] a) M. J. Natan, C. F. Millikan, J. G. Wright, T. V. Ohalloran, *J. Am. Chem. Soc.* **1990**, *112*, 3255–3257; b) R. A. Santos, E. S. Gruff, S. A. Koch, G. S. Harbison, *J. Am. Chem. Soc.* **1991**, *113*, 469–475.
[23] M. L. Zastrow, A. F. A. Peacock, J. A. Stuckey, V. L. Pecoraro, *Nat. Chem.* **2011**, *4*, 118–123.
[24] a) T. Butz, W. Troger, T. Pohlmann, O. Nuyken, *Z. Naturforsch. A* **1992**, *47*, 85–88; b) P. Faller, B. Ctortecka, W. Troger, T. Butz, M. Vasak, I. Collaboration, *J. Biol. Inorg. Chem.* **2000**, *5*, 393–401.
[25] L. Hemmingsen, K. N. Sas, E. Danielsen, *Chem. Rev.* **2004**, *104*, 4027–4061.
[26] L. Banci, I. Bertini, V. Calderone, N. Della-Malva, I. C. Felli, S. Neri, A. Pavelkova, A. Rosato, *Biochem. J.* **2009**, *422*, 37–42.
[27] D. Sheehan, *Physical Biochemistry: Principles and Applications*, Wiley–Blackwell, Chichester, **2009**, p. 407.
[28] Y. Goto, A. L. Fink, *Biochemistry* **1989**, *28*, 945–952.
[29] L. Banci, I. Bertini, S. Ciofi-Baffoni, T. Kozyreva, K. Zovo, P. Palumaa, *Nature* **2010**, *465*, 645–U145.
[30] B. A. Zeider, PhD Thesis, Western Michigan University (USA), **2010**.
[31] B. Wrackmeyer, R. Contreras, in *^{199}Hg NMR Parameters, Vol. 24* (Ed.: G. A. Webb), Academic Press, **1992**, pp. 267–329.
[32] G. L. Ellman, *Arch. Biochem. Biophys.* **1959**, *82*, 70–77.
[33] J. C. Cobas, F. J. Sardina, *Concepts Magn. Reson. Part A* **2003**, *19*, 80–96.
[34] T. Butz, S. Saibene, T. Fraenzke, M. Weber, *Nucl. Instrum. Methods Phys. Res. Sect. A* **1989**, *284*, 417–421.
[35] T. Butz, *Hyperfine Interact.* **1989**, *52*, 189–228.

Received: November 22, 2012
Revised: April 16, 2013
Published online: May 15, 2013

